

# Mitigating Object Hallucinations in Large Vision-Language Models via Attention Calibration

Younan Zhu<sup>1</sup> Linwei Tao<sup>1</sup> Minjing Dong<sup>2</sup> Chang Xu<sup>1</sup>

## Abstract

Large Vision-Language Models (LVLMs) exhibit impressive multimodal reasoning capabilities but remain highly susceptible to object hallucination, where models generate responses that are not factually aligned with the visual content. Recent works attribute this issue to an inherent bias of LVLMs where vision token attention map has a fixed correlation with spatial position, and propose to mitigate this issue by reordering visual tokens. However, we find that different LVLMs exhibit different correlations between attention and spatial position, which makes the existing solution difficult to generalize to other LVLMs. To address this issue, we first introduce a training-free solution, Uniform Attention Calibration (UAC), that estimates the bias from single meaningless input image and applies a calibration matrix to rectify attention imbalances. To further alleviate the bias, we relax the assumption of single meaningless input in UAC and introduce a fine-tuning solution, Dynamic Attention Calibration (DAC), that enforces the consistent outputs wherever the object locates in the image via a plug-and-play module. Comprehensive experiments across multiple benchmarks demonstrate that UAC and DAC significantly reduce object hallucination while improving general multimodal alignment. Our methods achieve state-of-the-art performance across diverse LVLM architectures on various metrics.

## 1. Introduction

Large Vision-Language Models (LVLMs) (Liu et al., 2024c; Bai et al., 2023; Dai et al., 2024; Zhu et al., 2023; Ye et al., 2024) have garnered significant attention in the AI research

<sup>1</sup>School of Computing Science, University of Sydney  
<sup>2</sup>Department of Computer Science, City University of Hong Kong.  
 Correspondence to: Chang Xu <c.xu@sydney.edu.au>.

*Proceedings of the 41<sup>st</sup> International Conference on Machine Learning*, Vancouver, Canada. PMLR 267, 2025. Copyright 2025 by the author(s).

community for their remarkable ability to comprehend the visual world and engage in conversational interactions with humans. Despite these advances, LVLMs continue to face critical challenges, particularly in the form of object hallucination (Li et al., 2023b; Rohrbach et al., 2018; Cui et al., 2023), a phenomenon where models generate responses that are not factually aligned with the visual content. This issue undermines the reliability of LVLMs, posing a significant barrier to their deployment in real-world applications.

A variety of approaches have been proposed to mitigate object hallucination in LVLMs. One common strategy involves post-hoc correction using revisor models (Yin et al., 2023; Zhou et al., 2024; Lee et al., 2023), which aim to reduce hallucinated responses by refining outputs. Another approach improves supervised fine-tuning through diversified instruction tuning data (Liu et al., 2024a; Yu et al., 2024) or aligns model responses with human preferences (Sun et al., 2023). Recently, several studies have explored training-free methods for mitigating object hallucination by addressing issues in the autoregressive decoding process of LVLMs (Leng et al., 2023; Huo et al., 2024; Huang et al., 2023).

A recent study (Xing et al., 2024) reveals that LVLMs' perception varies with object positions due to the inherent processing order in autoregressive models. As 2D vision tokens are concatenated with text tokens and flattened into a raster-scan sequence (top-to-bottom, left-to-right), the model develops a bias, prioritizing tokens in the bottom-right region closer to the instruction tokens (Figure 1a), termed as Spatial Perception Bias (SPB). This spatial bias skews perception capabilities. To mitigate this, Xing et al. (2024) propose a position alignment technique that reorders the perception sequence, reducing spatial bias.

However, this approach has two major limitations. First, the method is based on the assumption that the model assigns greater attention to tokens that are relatively nearby. As demonstrated in Figure 1(a-c), our analysis reveals that the attention distributions of vision tokens vary significantly across different LVLM models and unexpectedly high attentions are assigned to arbitrary locations. This observation challenges the generalization of the heuristic reordering strategy proposed by Xing et al. (2024), highlighting the need for a more dynamic and adaptable solution. Second,

the proposed technique requires retraining the entire network, which is computationally expensive and often impractical for large-scale LVLMs, underscoring the necessity of developing a lightweight alternative.

Building on this analysis, we aim to rectify the inherent SPB in vision token attention distributions. To achieve this, we introduce two attention calibration methods: Uniform Attention Calibration (UAC) and Dynamic Attention Calibration (DAC). UAC provides a simple training-free solution with competitive performance by calibrating biased attention through bias estimation on a meaningless input. Though effective and efficient, the performance of UAC could be limited due to the assumption of single meaningless input. Thus, we further relax the assumption in UAC and introduce DAC to fine-tune LVLMs for better performance. Specifically, DAC consists of a learnable plug-and-play module integrated into the self-attention mechanism. With a simple yet effective data augmentation technique, the module is then fine-tuned via contrastive learning to encourage consistent outputs with different object positions in the image, which dynamically adjusts vision token attention map to tackle object hallucination.

Comprehensive experiments confirm the effectiveness of UAC and DAC, revealing substantial improvements across multiple object hallucination benchmarks and a range of LVLMs, including LLaVA-1.5 (Liu et al., 2024c;b), mPLUG-Owl2 (Ye et al., 2024), and LLaVA-NeXT (Li et al., 2024). Additionally, our approach strengthens the overall perception capabilities of LVLMs, as demonstrated by its strong performance on MME (Fu et al., 2023) and LLaVA-Bench (Liu et al., 2024c), emphasizing its utility beyond mitigating object hallucination. To summarize, our main contributions are as follows:

1. We systematically investigate Spatial Perception Bias(SPB) in vision token attention within LVLMs, revealing its strong correlation with object hallucination and its persistence across different models.
2. Based on these findings, we propose Uniform Attention Calibration (UAC), a simple yet effective training-free bias correction module, and Dynamic Attention Calibration (DAC), a learnable plug-and-play module that dynamically adjusts vision token attention.
3. Extensive experiments confirm that both UAC and DAC significantly reduce object hallucination and enhance overall perception. Our methods achieve notable improvements across various LVLMs.

## 2. Related Work

### 2.1. Visual-Language Models

Large Vision-Language Models (LVLMs) have evolved from early BERT-based architectures (Devlin et al., 2018; Lu et al., 2019; Chen et al., 2019) to models that integrate Large Language Models (LLMs) (Bai et al., 2023; Brown et al., 2020; Gilardi et al., 2023; Raffel et al., 2020; Taori et al., 2023). Early vision-language models, such as ViLBERT (Lu et al., 2019) and LXMERT (Tan & Bansal, 2019), fused visual and textual features through transformer-based architectures. The introduction of LLMs enabled contrastive learning approaches like CLIP (Radford et al., 2021) and ALIGN (Jia et al., 2021), improving multimodal adaptability. Recent LVLMs, such as LLaVA (Liu et al., 2024c) and InstructBLIP (Dai et al., 2024), leverage visual instruction tuning for improved context-aware generation. Advances have further enabled referential dialogues (Chen et al., 2023a; You et al., 2023; Zhang et al., 2023a), interleaved image-text processing (Alayrac et al., 2022; Awadalla et al., 2023), and visual prompts (Peng et al., 2023; Zhang et al., 2023b; Chen et al., 2023b), broadening LVLM applications in interactive AI systems. These developments highlight a growing shift toward task-specific fine-tuning and multimodal interaction.

### 2.2. Hallucination in VLMs

Object hallucination arises when Large Vision-Language Models (LVLMs) generate textual descriptions containing objects or attributes not present in the accompanying image (Cui et al., 2023; Liu et al., 2024d; Guan et al., 2023; Li et al., 2023a; Wang et al., 2024; Nie et al., 2024). This phenomenon is frequently observed in tasks such as image captioning and visual question answering, where maintaining an accurate alignment between visual and textual content is critical. A range of methods has been proposed to address hallucination, from post-hoc correction using external or self-correcting models (Yin et al., 2023; Zhou et al., 2024; Lee et al., 2023) to enhanced instruction tuning that diversifies training data or aligns outputs with human feedback (Liu et al., 2024a; Yu et al., 2024; Sun et al., 2023). Recently, training-free approaches that rely on model-based distribution comparisons were proposed (Leng et al., 2023; Huo et al., 2024; Huang et al., 2023). As LVLMs grow more sophisticated and versatile, understanding and mitigating object hallucination remains a key focus in multimodal learning research. From a unique perspective, our design is rooted in the correlation between vision tokens attention and object hallucination.

## 3. Preliminary

In this section, we provide a brief overview of the widely adopted LVLMs architecture and explain how vision tokens

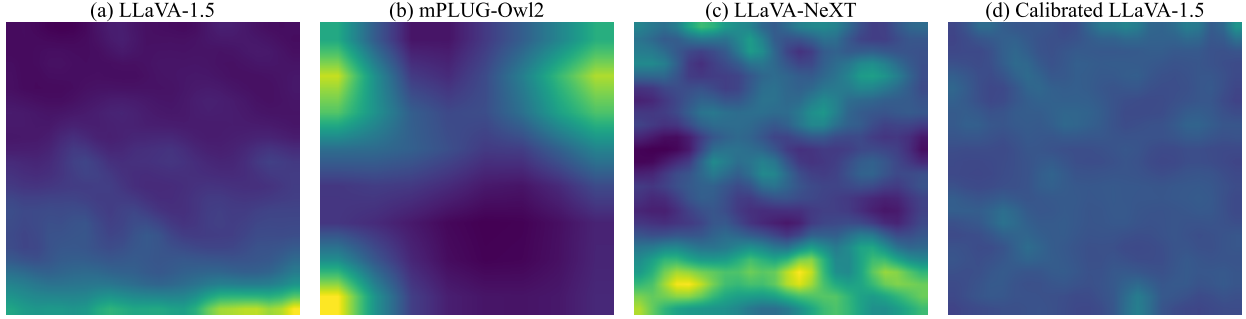


Figure 1: Spatial Position Bias influences how LVLMs perceive objects based on their position within an image. The visualization above illustrates vision tokens attention weights during the decoding process for different models on a blank white image in response to the open-ended prompt: “Please describe the image in detail.” (a) shows LLaVA-1.5, which exhibits an increasing trend in attention distribution following a raster scan order, as identified by (Xing et al., 2024). (b-c) represent other models, displaying arbitrary attention distributions. (d) depicts the calibrated vision tokens attention map of LLaVA-1.5 after Dynamic Attention Calibration.

are involved in the self attention module. Additionally, we review the how LVLMs exhibit spatial perception bias problem, highlighting systematic biases that affect LVLM hallucination.

### 3.1. LVLMs: Generation and Attention Mechanism

**Vision and Language Inputs** LVLMs process both image  $v$  and text  $t$  inputs. Raw images are divided into patches and encoded by a visual encoder, followed by a cross-modal projection module that maps visual features into the token space. This yields a sequence of vision tokens  $v = \{v_i \mid i = 1, 2, \dots, n\}$ , where  $n$  is the number of vision tokens. Text inputs are tokenized and embedded into text tokens  $t = \{t_j \mid j = 1, 2, \dots, m\}$ , where  $m$  is the number of text tokens. The vision and text tokens are then concatenated into a unified input sequence  $x = \{v, t\}$ , ensuring a shared multimodal representation space, with  $v_i, t_j \in \mathbb{R}^d$ , where  $d$  denotes the feature dimensionality.

**Language Model Generation** LVLMs are typically built on pre-trained LLMs such as Vicuna (Chiang et al., 2023) or LLaMA (Touvron et al., 2023), parameterized by  $\theta$ . The model takes a input  $x$  and predicts the next token probability  $p(y_i)$  at time step  $i$  in an autoregressive manner:

$$p(y_i \mid x, y_{<i}) = \text{softmax}(\text{logit}_\theta(y_i \mid x, y_{<i})) \quad (1)$$

**Self-Attention Mechanism** The self-attention mechanism computes token relevance by projecting the output of previous layer into query  $Q$ , key  $K$ , and value  $V$  with linear transformations  $W_Q, W_K, W_V$ . The self attention output is computed as

$$\text{SA}(Q, K, V) = \text{softmax}(\mathbf{A} + M) \cdot V, \quad \mathbf{A} = \frac{Q \cdot K^T}{\sqrt{d_l}}, \quad (2)$$

where  $\mathbf{A} \in \mathbb{R}^{B \times H \times (n+m) \times (n+m)}$ <sup>1</sup> denotes attention weight matrix,  $B$  and  $H$  represent the batch size, and number of attention heads, respectively.  $M$  denotes the causal mask, and  $d_l$  is the dimensionality of  $Q, K$ , and  $V$ . We denote  $\mathbf{A}^i$  as the attention matrix after  $i$ -th layer of LVLM, In this paper, we denote vision tokens attention  $\mathbf{A}_{\text{img}} \in \mathbb{R}^{B \times H \times n}$  as the slice of the attention weights corresponding to the vision token inputs  $v$ .

### 3.2. Spatial Perception Bias

When given a blank white image and the open-ended prompt “Please describe the image in detail,” LVLMs are expected to distribute attention uniformly across the entire image. However, as shown in Figure 1a, the self-attention module assigns varying levels of attention to different spatial regions. For instance, LLaVA-1.5 places greater attention on later visual tokens, particularly near the bottom-right. This systematic attention bias reflects position-dependent sensitivity to visual features. We define this phenomenon as Spatial Perception Bias(SPB)—a systematic error in the self-attention module that skews attention weights.

Xing et al. (2024) were the first to identify a similar issue, attributing it to the long-term decay effect of position encoding. Specifically, LVLMs tend to assign lower attention to top-left tokens compared to bottom-right tokens. To mitigate this, they proposed reordering the visual token sequence to achieve a more balanced attention distribution. However, when comparing Figure 1(a–c), we find that SPB varies significantly across models and can result in unexpectedly high attention to arbitrary locations. Consequently, a predefined token reordering strategy (Xing et al., 2024) may not generalize well to LVLMs beyond LLaVA-1.5.

<sup>1</sup>We omit the system tokens for simplicity.

## 4. Method

A valid approach to mitigating bias is to calibrate the attention values. Since the attention map essentially forms a discrete probability distribution that sums to one, this problem closely resembles uncertainty calibration (Guo et al., 2017). A common strategy in uncertainty calibration literature is to adjust the probability distribution by modifying the output logits. Inspired by calibration literature, we propose two attention calibration techniques to meet different needs: **Uniform Attention Calibration (UAC)** and **Dynamic Attention Calibration (DAC)**. UAC is a training-free method that removes SPB estimated from a meaningless input, offering a simple yet effective solution with competitive performance. In addition, DAC is a learnable plug-and-play module within the self-attention mechanism, providing state-of-the-art performance with minimal computational overhead.

### 4.1. Uniform Attention Calibration

We hypothesize that LVLMs should assign uniform attention to meaningless images, such as blank white or random noise images. Therefore, we introduce UAC, which enforces uniform attention by first estimating SPB from a meaningless input (defaulting to a blank white image) and computing a calibration matrix  $W$  that adjusts vision tokens attention map to be uniform across all positions. This matrix is then applied as an affine transformation to vision tokens attention during inference.

Specifically, we first obtain the attention map  $\tilde{\mathbf{A}}_{\text{img}}$  for a meaningless input and compute calibration matrix  $W$  as:

$$W = \frac{\text{avg}(\tilde{\mathbf{A}}_{\text{img}})}{\tilde{\mathbf{A}}_{\text{img}}} \quad (3)$$

where  $\text{avg}(\cdot)$  denotes the average value over all elements.

During inference, the calibrated attention matrix  $\mathbf{A}'_{\text{img}}$  for any input image is obtained as:

$$\mathbf{A}'_{\text{img}} = W \circ \mathbf{A}_{\text{img}} \quad (4)$$

where  $\mathbf{A}_{\text{img}}$  represents the original attention weights computed from the input image,  $\circ$  denotes the element-wise (Hadamard) product. Notably,  $W$  can be calculated and applied to any layer of the LVLM decoder, making it a flexible and model-agnostic calibration method.

### 4.2. Dynamic Attention Calibration

UAC removes SPB by assuming a single meaningless reference, but this one-size-fits-all approach does not guarantee optimal attention calibration across diverse inputs. To overcome this limitation, we seek an trainable solution that allows LVLMs to dynamically adjust their attention

distributions while ensuring invariance to an object’s spatial position within an image. To this end, we introduce Dynamic Attention Calibration (DAC), which involves plug-and-play learnable module to dynamically calibrate the SPB via contrastive learning (Wu et al., 2018; Chen et al., 2020).

**DAC Design** Motivated by the superior calibration performance of affine transformation in the field of uncertainty calibration (Platt, 1999), we introduce a lightweight trainable transformation  $f$  to calibrate unreliable vision token attention weights before SoftMax function as  $\mathbf{A}'_{\text{img}} = f(\mathbf{A}_{\text{img}})$ , where  $\mathbf{A}'_{\text{img}}$  denotes the calibrated vision token attention weights. Specifically, the transformation  $f$  operates within the self-attention mechanism of the transformer decoder layers and consists of a small stack of linear transformations with ReLU activations. The details about building blocks can be found in the Appendix. The forward pass of DAC module can be defined as

$$\begin{aligned} \mathbf{A}'_{\text{img}} &= f(\mathbf{A}_{\text{img}}) = \mathbf{g}_{L-1} \mathbf{W}_L + \mathbf{b}_L, \\ \mathbf{g}_i &= \text{ReLU}(\mathbf{g}_{i-1} \mathbf{W}_i + \mathbf{b}_i), \text{ for } i \in \{1, \dots, N-1\}, \end{aligned} \quad (5)$$

where  $L$  denotes the layer number in DAC module,  $\mathbf{W}_i \in \mathbb{R}^{D_i \times D_i}$  denotes the weight matrix of layer  $i$ ,  $\mathbf{b}_i \in \mathbb{R}^{D_i}$  denotes the bias vector,  $\mathbf{g}_i$  represents the output of the  $i$ -th layer, and  $\mathbf{g}_0 = \mathbf{A}_{\text{img}}$ . The DAC module can be applied to any layer of the language model decoder, targeting the layers responsible for vision tokens processing.

**DAC Optimization** With the DAC module in Eq. 5, a much stronger constraint can be imposed on vison token attention weights of LVLMs to alleviate the bias. Instead of the uniform constraint in UAC, we further propose to force the consistent outputs wherever the object locates in the image. The key idea is to ensure that the model maintains the same capability of identifying an object regardless of its position within the image. However, to impose such a constraint, it could be challenging to obtain sufficient training data variants with different object positions. Thus, we introduce a simple yet effective data augmentation technique inspired by the concept of instant discrimination (Wu et al., 2018; Chen et al., 2020).

Formally, we select a small portion of the validation set, 20% of the total validation data, as our calibration set, denoted as  $\mathcal{D}_{\text{cal}}$ . Each image  $V \in \mathcal{D}_{\text{cal}}$  is paired with ground-truth annotations and their corresponding bounding boxes. The calibration set  $\mathcal{D}_{\text{cal}}$  undergoes an augmentation process to produce the augmented dataset  $\mathcal{D}_{\text{aug}}$ . Specifically, we crop the ground truth objects from the images using the annotations and bounding boxes provided, then apply random resizing and paste the cropped objects onto a pure white background as  $V_{\text{crop}}$ . For each  $V_{\text{crop}}$ , we generate balanced positive and negative query-label pairs, ensuring a well-balanced dataset. Additionally, we include annotations for

the cropped images  $V_{\text{crop}}$  to be utilized in instance discrimination tasks, as discussed later in the paper. The detailed augmentation process is summarized in the Appendix.

With sufficient augmented data from  $\mathcal{D}_{\text{aug}}$ , we propose leveraging contrastive learning to encourage LVLMs to focus on objects themselves rather than their absolute positions in the image. This approach ensures consistent outputs regardless of object position. By reducing reliance on positional cues, the model learns to robustly identify objects despite spatial transformations. Specifically, contrastive learning is formulated to increase the similarity between embeddings of the same object at different spatial locations while pushing apart the embeddings of different objects. We begin with an  $\mathcal{D}_{\text{aug}}$  dataset and randomly sample a minibatch of  $B$  examples. Each example then undergoes an additional augmentation process, resulting in a total of  $2B$  augmented data points. Following the approach of (Wu et al., 2018), for each positive pair, we consider the remaining  $2(B-1)$  augmented examples within the minibatch as negative examples. Given the embeddings  $z_i$  and  $z_j$  of the positive augmented pair  $\tilde{v}_i$  and  $\tilde{v}_j$ , the contrastive loss can be expressed as:

$$\ell_{\text{CL}}(i, j) = -\log \frac{\exp(\text{sim}(z_i, z_j)/\tau)}{\sum_{k=1}^{2B} \mathbb{1}[k \neq i] \exp(\text{sim}(z_i, z_k)/\tau)}, \quad (6)$$

where  $B$  denotes the number of examples in a minibatch,  $\text{sim}(\cdot, \cdot)$  represents the cosine similarity,  $\mathbb{1}[k \neq i]$  is an indicator function, and  $\tau$  is the temperature parameter. Combined with a cross-entropy (CE) loss, the final loss function is formulated as

$$\mathcal{L} = \mathcal{L}_{\text{CE}}(F(T_{\text{crop}}, V_{\text{crop}}), Y_{\text{crop}}) + \lambda \mathcal{L}_{\text{CL}}, \quad (7)$$

where  $F$  represents the model,  $T_{\text{crop}}$  and  $V_{\text{crop}}$  are the query and cropped image,  $Y_{\text{crop}}$  is the corresponding label, and  $\lambda$  is a hyperparameter balancing the two losses. We optimize our DAC using Eq. 7 alongside instruction tuning, while keeping all other components frozen. The overall training process is summarized in Algorithm 1.

## 5. Experiment

### 5.1. Setup

**Models and Baselines** We implement three representative LVLMs for evaluation: LLaVA-1.5 (Shang et al., 2024) and mPLUG-Owl2 (Ye et al., 2024) at the 7B scale, and LLaVA-NeXT (Li et al., 2024) at the 8B scale. Our method is compared against five methods. Baseline responses are generated using the original LVLMs, while other techniques such as Visual Contrastive Decoding (VCD) (Leng et al., 2023), OPERA (Huang et al., 2023), Self-Introspective Decoding (SID) (Huo et al., 2024), and Concentric Causal Attention (CCA) (Xing et al., 2024) are included for comparative analysis. Additional details on the compared methods are provided in the Appendix.

---

**Algorithm 1** DAC’s Main Learning Algorithm

---

**Input:** Batch size  $B$ , constant  $\tau$ , frozen backbone networks  $f(\cdot)$  and projection head  $g(\cdot)$ , augmentation distribution  $\mathcal{T}$ , augmented set  $\mathcal{D}_{\text{aug}} = \{(T_{\text{aug}}, V_{\text{crop}}, Y_{\text{aug}})\}$   
**for** sampled minibatch  $\{(t_k, v_k, y_k)\}_{k=1}^B \in \mathcal{D}_{\text{aug}}$  **do**  
    **for** all  $k \in \{1, \dots, B\}$  **do**  
        Draw one augmentation function  $t \sim \mathcal{T}$   
        # Original augmentation  
         $\tilde{v}_{2k-1} = v_k$  # Representation  
         $\tilde{z}_{2k-1} = f(\tilde{v}_{2k-1})$  # Prediction  
         $\tilde{y}_{2k-1} = g(\tilde{z}_{2k-1})$  # Label  
         $y_{2k-1} = y_k$  # The second augmentation  
         $\tilde{v}_{2k} = t(v_k)$  # Representation  
         $\tilde{z}_{2k} = f(\tilde{v}_{2k})$  # Prediction  
         $\tilde{y}_{2k} = g(\tilde{z}_{2k})$  # Label  
         $y_{2k} = y_k$   
    **end for**  
    **for** all  $i \in \{1, \dots, 2B\}$  and  $j \in \{1, \dots, 2B\}$  **do**  
         $s_{i,j} = z_i^\top z_j / (\|z_i\| \|z_j\|)$  # Pairwise similarity  
    **end for**  
    Compute the losses using:  

$$\mathcal{L} = \mathcal{L}_{\text{CE}} + \lambda \cdot \mathcal{L}_{\text{CL}}$$
  
    Update DAC parameters to minimize  $\mathcal{L}$   
**end for**  
**Return:** Fine-tuned DAC

---

**Experiment Settings** Unless otherwise specified, we integrate the DAC module into two consecutive layers of the language model decoder. For the POPE COCO dataset, we select 20% of the validation set, comprising 100 images, as our calibration set  $D_{\text{cal}}$  and report results on the remaining 80% of the validation set. The optimal layers are determined based on performance on  $D_{\text{cal}}$ . For other datasets, we report results trained on the POPE COCO Random dataset. For each image, we select up to three ground truth objects; if an image contains fewer than three objects, all available objects are included. Using these ground truth objects, we generate 10 cropped images per object, resulting in a dataset of approximately 5.4K  $(T, V, Y)$  pairs. By default, the contrastive loss strength  $\lambda$  is set to 0.01.

We fine-tune our module on LLaVA-1.5 on the proposed  $\mathcal{D}_{\text{aug}}$  dataset using a learning rate of  $3 \times 10^{-6}$  and a batch size of 8, and gradient accumulate steps of 4. The training is conducted on two NVIDIA RTX 4090 GPUs with approximately 40 minutes. See Appendix for additional training details.

Setting			Random		Popular		Adversarial	
Dataset	Model	Method	Accuracy↑	F1 Score↑	Accuracy↑	F1 Score↑	Accuracy↑	F1 Score↑
LLaVA1.5	mPLUG-Owl2	Baseline	89.41	89.32	85.33	85.77	78.92	80.75
		VCD	87.53	87.81	84.43	85.20	78.13	80.38
		OPERA	89.87	89.95	86.30	86.88	79.77	81.77
		SID	89.38	89.00	85.45	85.01	80.25	81.28
		CCA	89.77	89.05	86.45	86.02	83.97	83.82
		DAC	<b>90.83</b>	<b>90.60</b>	<b>89.50</b>	<b>89.10</b>	<b>84.12</b>	<b>84.42</b>
MSCOCO	mPLUG-Owl2	Baseline	86.27	86.88	80.73	82.52	76.17	77.69
		VCD	84.40	84.79	81.00	81.12	77.10	77.00
		OPERA	86.23	86.84	80.70	82.48	76.87	78.01
		SID	86.13	86.69	81.20	82.77	77.25	79.84
		DAC	<b>87.71</b>	<b>87.57</b>	<b>84.96</b>	<b>84.46</b>	<b>82.58</b>	<b>82.32</b>
	LLaVA-NeXT	Baseline	89.37	88.82	83.68	84.62	80.08	80.74
		VCD	87.83	87.09	82.68	83.55	79.61	81.20
		OPERA	89.36	88.80	83.65	84.60	80.10	80.75
		SID	90.05	89.97	86.13	85.69	84.06	82.95
		DAC	<b>90.33</b>	<b>90.71</b>	<b>88.25</b>	<b>87.69</b>	<b>84.38</b>	<b>84.38</b>
A-OKVQA	mPLUG-Owl2	Baseline	87.30	88.49	80.30	83.21	69.33	76.10
		VCD	85.00	86.49	77.50	81.07	67.90	75.01
		OPERA	87.27	88.50	80.47	83.38	69.20	76.09
		SID	86.92	87.64	81.63	83.46	72.24	70.08
		CCA	<b>90.00</b>	90.11	<b>85.45</b>	85.01	74.77	78.32
		DAC	89.70	<b>90.33</b>	83.96	<b>85.52</b>	<b>75.42</b>	<b>79.21</b>
	LLaVA-NeXT	Baseline	81.57	83.89	75.97	79.98	67.37	74.63
		VCD	82.53	84.16	75.70	79.21	68.80	74.85
		OPERA	81.53	83.86	75.93	79.94	67.30	74.58
		SID	86.13	84.98	77.21	80.69	68.51	75.12
		DAC	<b>86.56</b>	<b>87.24</b>	<b>82.83</b>	<b>83.47</b>	<b>75.88</b>	<b>77.78</b>

Table 1: POPE results. Results are sourced from published papers or re-implemented using official code. The best performance within each setting is highlighted in **bold**.

## 5.2. Evaluation Results

**POPE** Polling-based Object Probing Evaluation (POPE) (Li et al., 2023b) is a method designed to assess object hallucination in Large Vision-Language Models (LVLMs). It evaluates model performance by querying the presence of specific objects in images using yes-or-no questions. POPE employs three strategies for sampling negative objects: Random, Popular, and Adversarial (refer to (Li et al., 2023b) for details). Our evaluation utilizes two datasets: COCO (Lin et al., 2014) and A-OKVQA (Schwenk et al., 2022). For each evaluation setup, every subset includes 3,000 questions

across 500 images, resulting in a total of 18,000 yes-or-no questions. The evaluation pivots on two key metrics: Accuracy and the F1 score. Our method achieves the highest accuracy and F1 scores across most datasets and sampling setups, as shown in Table 1. Specifically, DAC delivers an average improvement of 1.36% in accuracy and 1.90% in F1 score for Random sampling, 2.96% in accuracy and 2.39% in F1 score for Popular sampling, and 3.39% in accuracy and 2.22% in F1 score for Adversarial sampling, compared to the next best approach. Our method achieves more significant improvements in the more challenging Adversarial sampling setting because it effectively downplays visual

Setting	LLaVA1.5		LLaVA-NeXT	
	$C_S \downarrow$	$C_I \downarrow$	$C_S \downarrow$	$C_I \downarrow$
Baseline	51.3	16.8	42.6	14.1
VCD	48.0	14.3	41.3	12.9
OPERA	45.2	12.7	39.4	11.8
SID	45.0	<b>11.7</b>	38.4	11.4
CCA	48.6	13.4	-	-
DAC	<b>30.8</b>	12.7	<b>21.4</b>	<b>10.2</b>

Table 2: CHAIR results on 500 randomly sampled MSCOCO images with a maximum sequence length of 512 tokens. The best performance within each setting is highlighted in **bold**.

Setting	Object-level $existence \uparrow count \uparrow$	Attribute-level $position \uparrow color \uparrow$	Total $\uparrow$
Baseline	175.67	124.67	114.00 151.00 565.33
VCD	184.66	138.33	128.67 153.00 604.66
OPERA	180.67	133.33	123.33 155.00 592.33
SID	190.00	148.33	128.33 <b>175.00</b> 641.66
CCA	190.00	148.33	128.33 <b>175.00</b> 641.66
DAC	<b>195.00</b>	<b>158.33</b>	<b>133.33</b> 170.00 <b>656.67</b>

Table 3: MME hallucination subset results. The best performance within each setting is highlighted in **bold**.

cues unrelated to the object itself.

**CHAIR** The Caption Hallucination Assessment with Image Relevance (CHAIR) metric (Rohrbach et al., 2018) is specifically designed to assess object hallucinations in image captioning tasks. CHAIR quantifies the degree of hallucinations in a generated image caption by calculating the proportion of objects mentioned in the caption that are not present in the ground truth label pool. Two common variants of CHAIR are defined:  $CHAIR_S$  ( $C_S$ ) and  $CHAIR_I$  ( $C_I$ ), which measure hallucination at the instance and sentence levels, respectively. These metrics are formulated as follows:

$$C_S = \frac{|\text{hallucinated objects}|}{|\text{all mentioned objects}|}, \quad C_I = \frac{|\text{captions with hallucinated objects}|}{|\text{all captions}|}$$

Lower values of  $C_S$  and  $C_I$  indicate better performances. Following (Huang et al., 2023; Huo et al., 2024), we randomly select 500 images from the validation set of COCO 2014 and query various LVLMs using the prompt: “*Please describe this image in detail.*” To ensure a fair evaluation, we limit the maximum number of new tokens to 512 when generating descriptions. As shown in Table 2, our method, DAC, consistently outperforms other methods in most cases. Notably, on  $CHAIR_S$ , DAC achieves a significant improvement, reducing the hallucination rate by an average of 37.07% across models compared to the next best

approach. The superior performance of DAC on CHAIR metrics showcases its capability to effectively mitigate hallucinations in open-ended generation settings.

**MME** The MME benchmark (Fu et al., 2023) provides a comprehensive framework for evaluating LVLMs across multiple dimensions. It includes ten perception-related sub-tasks and four cognition-focused tasks. Following (Leng et al., 2023; Yin et al., 2023), we evaluate four perception subtasks that assess object-level and attribute-level hallucinations, specifically measuring object existence, count, position, and color. Table 3 presents the performance of our method, DAC, on the MME hallucination subset using LLaVA-1.5. DAC achieves a notable improvement of 16.16% over the baseline and 2.34% over the current state-of-the-art hallucination mitigation approaches, demonstrating its effectiveness in enhancing the general perception capabilities of LVLMs. Detailed results for the full MME benchmark are provided in the Appendix.

**GPT4V-Aided Evaluation** We evaluate our approach on LLaVA-Bench (Liu et al., 2024c), a benchmark comprising 30 images paired with a total of 90 questions. LLaVA-Bench is designed to assess the ability of models to generate coherent and contextually accurate responses for vision-language tasks. It categorizes questions into three types: conversation, detailed description, and complex reasoning. Following prior works (Liu et al., 2024c; Huang et al., 2023), we prompt these models to generate responses and use the text-only GPT-4 (Achiam et al., 2023) as the judge to rate these responses. The results on LLaVA-1.5 are presented in Table 4. Our method demonstrates strong performance across all question type. These results highlight the effectiveness of our approach at preserving language understanding and generation capabilities while significantly mitigating object hallucination.

**Uniform Attention Calibration results** To address the SPB inherent in LVLMs, we propose a training-free method UAC in Sec. 4.1. UAC recalibrates biased attention by estimating SPB from a meaningless input. We evaluate this method using LLaVA-1.5 on the POPE MSCOCO, CHAIR, and MME benchmarks, following the same experimental setup as in our other comparisons. As summarized in 5, UAC achieves the best overall performance on POPE MSCOCO compared to current state-of-the-art methods, surpassing other training-free approaches by a substantial margin. On the MME dataset, UAC attains competitive results. However, on the open-ended generation benchmark CHAIR, UAC falls short of the top performers. We attribute this to its reliance on a single meaningless image bias for calibration, which, while effective for structured tasks, may degrade generation quality in open-ended settings by limiting the model’s ability to adapt to diverse contextual vari-

Method	Complex↑	Details↑	Conv↑	Average↑
Baseline	66.3	46.7	68.7	60.6
VCD	69.6	51.6	57.3	61.6
OPERA	66.4	<b>56.9</b>	44.0	61.3
SID	66.7	51.3	66.3	60.4
CCA	66.1	53.9	69.4	<b>64.3</b>
DAC	<b>70.3</b>	50.0	<b>72.7</b>	<b>64.3</b>

Table 4: LLaVA-Bench results. The results are reimplemented using the official code and evaluated with the latest available text-only GPT-4 API. Scores are normalized by the total possible score. The best performances within each setting are highlighted in **bold**.

Setting	POPE MSCOCO			CHAIR		MME↑
	Rnd↑	Pop↑	Adv↑	$C_S \downarrow$	$C_i \downarrow$	
Baseline	89.3	85.8	80.8	51.3	16.8	565.3
VCD	87.8	85.2	80.4	48.0	14.3	604.7
OPERA	90.0	86.9	81.8	45.2	12.7	592.3
SID	89.0	85.0	81.3	45.0	<b>11.7</b>	641.7
CCA	89.1	86.0	83.8	48.6	13.4	641.7
UAC	90.2	87.6	83.7	49.0	14.9	638.3
DAC	<b>90.6</b>	<b>89.1</b>	<b>84.4</b>	<b>30.8</b>	12.7	<b>656.7</b>

Table 5: Results on POPE MSCOCO, CHAIR, and MME hallucination subsets. “Rnd” “Pop” and “Adv” represent the Random, Popular, and Adversarial settings, respectively. On POPE MSCOCO, results are reported as F1 scores. The best performances within each settings are highlighted in **bold**.

ations. Notably, UAC incurs no inference overhead since its parameters remain fixed across all tasks. In contrast, other training-free methods, including VCD, OPERA, and SID, impose significant inference costs—approximately  $2\times$ ,  $5\times$ , and  $1.7\times$ , respectively (Huo et al., 2024). These results highlight UAC as an effective and efficient solution for structured tasks, while DAC continues to provide state-of-the-art performance with minimal computational overhead.

### 5.3. Ablation Study

In this section, we present a detailed ablation study on key hyperparameters, focusing on two critical components: the contrastive loss strength  $\lambda$  and the decoder layers  $N_{DAC}$  to which DAC is applied. As shown in Figure 2, DAC exhibits robustness across various settings and consistently outperforms the baseline.

To maintain effective language generation, we avoid setting  $\lambda$  too large, as excessively high values lead to degradation in the model’s generative capabilities. Conversely, when  $\lambda = 0$ , meaning the model is fine-tuned solely on the CE

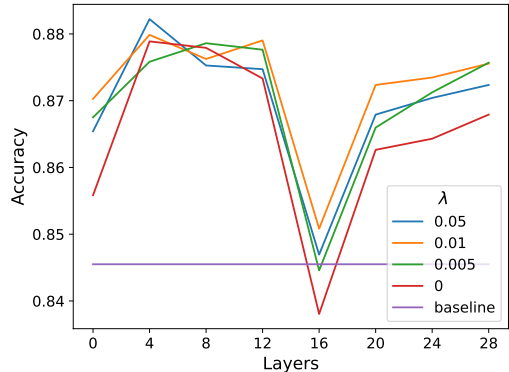


Figure 2: DAC performance under different settings of  $\lambda$  and  $N_{DAC}$ . Different lines represent various  $\lambda$  values, while the y-axis indicates  $N_{DAC}$ . DAC is applied to 2 consecutive layers, and the results average sampling settings for POPE accuracy using LLaVA1.5-7B.

loss, it yields the lowest performance among the tested settings. This result highlights the importance of the contrastive learning component. Our experiments indicate that  $\lambda = 0.01$  achieves the best performance, with further adjustments yielding negligible differences. For simplicity and consistency, we adopt  $\lambda = 0.01$  throughout this study.

DAC demonstrates significant improvements across various layer configurations. Following established calibration practices (Guo et al., 2017; Mukhoti et al., 2020), we train DAC using the augmented dataset  $D_{aug}$  and utilize the calibration dataset  $D_{cal}$  as the validation set to determine the optimal  $N_{DAC}$ , thereby preventing data leakage.

## 6. Conclusion and Limitation

In this paper, we investigated object hallucination in LVLMs and identified an inherent imbalance in vision token attention within these models, particularly in spatial positioning, as a key contributing factor. Our findings highlight that such imbalances amplify SPB, thereby increasing the likelihood of hallucinations. To address this challenge, we introduced Uniform Attention Calibration (UAC) and Dynamic Attention Calibration (DAC), two efficient techniques designed for vision token attention correction. UAC offers a training-free solution that estimates SPB using a meaningless input and applies a calibration matrix to mitigate attention imbalances. DAC, on the other hand, is a learnable module that dynamically refines attention weights within the self-attention mechanism. Through extensive evaluations on multiple benchmarks and LVLM architectures, our methods consistently reduce hallucination while improving general perception. These results emphasize the significance of attention calibration in enhancing LVLM reliability

and performance, providing a promising direction for future research in mitigating hallucination-related biases.

**Limitation** Although this study employs a data-efficient approach to introducing SPB, its effectiveness may be limited when validation data is scarce. A promising direction for future work is the development of fine-grained, data-free calibration techniques and extend the idea of attention calibration to improve spatial perception in LVLMs.

## References

Achiam, J., Adler, S., Agarwal, S., Ahmad, L., Akkaya, I., Aleman, F. L., Almeida, D., Altenschmidt, J., Altman, S., Anadkat, S., et al. Gpt-4 technical report. *arXiv preprint arXiv:2303.08774*, 2023.

Alayrac, J.-B., Donahue, J., Luc, P., Miech, A., Barr, I., Hasson, Y., Lenc, K., Mensch, A., Millican, K., Reynolds, M., et al. Flamingo: A visual language model for few-shot learning. *Advances in Neural Information Processing Systems*, 35:23716–23736, 2022.

Awadalla, A., Gao, I., Gardner, J., Hessel, J., Hanafy, Y., Zhu, W., Marathe, K., Bitton, Y., Gadre, S., Sagawa, S., et al. Openflamingo: An open-source framework for training large autoregressive vision-language models. *arXiv preprint arXiv:2308.01390*, 2023.

Bai, J., Bai, S., Chu, Y., Cui, Z., Dang, K., Deng, X., Fan, Y., Ge, W., Han, Y., Huang, F., et al. Qwen technical report. *arXiv preprint arXiv:2309.16609*, 2023.

Brown, T., Mann, B., Ryder, N., Subbiah, M., Kaplan, J. D., Dhariwal, P., Neelakantan, A., Shyam, P., Sastry, G., Askell, A., et al. Language models are few-shot learners. In *Advances in Neural Information Processing Systems (NeurIPS)*, volume 33, pp. 1877–1901, 2020.

Chen, K., Zhang, Z., Zeng, W., Zhang, R., Zhu, F., and Zhao, R. Shikra: Unleashing multimodal llm’s referential dialogue magic. *arXiv preprint arXiv:2306.15195*, 2023a.

Chen, T., Kornblith, S., Norouzi, M., and Hinton, G. A simple framework for contrastive learning of visual representations. In *International Conference on Machine Learning*, pp. 1597–1607. PMLR, 2020.

Chen, W.-G., Spiridonova, I., Yang, J., Gao, J., and Li, C. Llava-interactive: An all-in-one demo for image chat, segmentation, generation and editing. *arXiv preprint arXiv:2311.00571*, 2023b.

Chen, Y.-C., Li, L., Yu, L., Kholy, A. E., Ahmed, F., Gan, Z., Cheng, Y., and Liu, J. Uniter: Learning universal image-text representations. *arXiv preprint arXiv:1909.11740*, 2019.

Chiang, W.-L., Li, Z., and et al. Vicuna: An open-source chatbot impressing gpt-4 with 90% chatgpt quality, 2023. See <https://vicuna.lmsys.org> (accessed 14 April 2023).

Cui, C., Zhou, Y., Yang, X., Wu, S., Zhang, L., Zou, J., and Yao, H. Holistic analysis of hallucination in gpt-4v (ision): Bias and interference challenges. *arXiv preprint arXiv:2311.03287*, 2023.

Dai, W., Li, J., Li, D., Tiong, A. M. H., Zhao, J., Wang, W., Li, B., Fung, P. N., and Hoi, S. Instructblip: Towards general-purpose vision-language models with instruction tuning. *Advances in Neural Information Processing Systems*, 36, 2024.

Devlin, J., Chang, M.-W., Lee, K., and Toutanova, K. BERT: Pre-training of Deep Bidirectional Transformers for Language Understanding. *arXiv preprint arXiv:1810.04805*, 2018.

Fu, C., Chen, P., and et al. Mme: A comprehensive evaluation benchmark for multimodal large language models. *arXiv preprint arXiv:2306.13394*, 2023.

Gilardi, F., Alizadeh, M., and Kubli, M. Chatgpt outperforms crowd-workers for text-annotation tasks. *arXiv preprint arXiv:2303.15056*, 2023.

Guan, T., Liu, F., Wu, X., Xian, R., Li, Z., Liu, X., Wang, X., Chen, L., Huang, F., Yacoob, Y., et al. Hallusionbench: An advanced diagnostic suite for entangled language hallucination & visual illusion in large vision-language models. *arXiv preprint arXiv:2310.14566*, 2023.

Guo, C., Pleiss, G., Sun, Y., and Weinberger, K. Q. On calibration of modern neural networks. In *Proceedings of the 34th International Conference on Machine Learning (ICML)*, volume 70, pp. 1321–1330. PMLR, 2017.

Huang, Q., Dong, X., Zhang, P., Wang, B., He, C., Wang, J., Lin, D., Zhang, W., and Yu, N. Opera: Alleviating hallucination in multi-modal large language models via over-trust penalty and retrospection-allocation. *arXiv preprint arXiv:2311.17911*, 2023.

Huo, F., Xu, W., Zhang, Z., Wang, H., Chen, Z., and Zhao, P. Self-introspective decoding: Alleviating hallucinations for large vision-language models. *arXiv preprint arXiv:2408.02032*, 2024.

Jia, C., Yang, Y., Xia, Y., Chen, Y.-T., Parekh, Z., Pham, H., Le, Q., Sung, Y.-H., Li, Z., and Duerig, T. Scaling up visual and vision-language representation learning with noisy text supervision. In *International Conference on Machine Learning (ICML)*, pp. 4904–4916. PMLR, 2021.

Langley, P. Crafting papers on machine learning. In Langley, P. (ed.), *Proceedings of the 17th International Conference on Machine Learning (ICML 2000)*, pp. 1207–1216, Stanford, CA, 2000. Morgan Kaufmann.

Lee, S., Park, S. H., Jo, Y., and Seo, M. Volcano: Mitigating multimodal hallucination through self-feedback guided revision. *arXiv preprint arXiv:2311.07362*, 2023.

Leng, S., Zhang, H., Chen, G., Li, X., Lu, S., Miao, C., and Bing, L. Mitigating object hallucinations in large vision-language models through visual contrastive decoding. *arXiv preprint, arXiv:2311.16922*, 2023.

Li, B., Zhang, K., and et al. Llava-next: Stronger llms supercharge multimodal capabilities in the wild, May 2024. URL <https://llava-vl.github.io/blog/2024-05-10-llava-next-stronger-llms/>.

Li, Y., Du, Y., Zhou, K., Wang, J., Zhao, W. X., and Wen, J.-R. Evaluating object hallucination in large vision-language models. *arXiv preprint arXiv:2305.10355*, 2023a.

Li, Y., Du, Y., Zhou, K., Wang, J., Zhao, W. X., and Wen, J.-R. Evaluating object hallucination in large vision-language models. *arXiv preprint, arXiv:2305.10355*, 2023b.

Lin, T.-Y., Maire, M., Belongie, S., Hays, J., Perona, P., Ramanan, D., Dollár, P., and Zitnick, C. L. Microsoft coco: Common objects in context. In *Computer Vision–ECCV 2014: 13th European Conference, Zurich, Switzerland, September 6–12, 2014, Proceedings, Part V*, volume 8693 of *Lecture Notes in Computer Science*, pp. 740–755. Springer, 2014.

Liu, F., Lin, K., Li, L., Wang, J., Yacoob, Y., and Wang, L. Mitigating hallucination in large multi-modal models via robust instruction tuning. In *The Twelfth International Conference on Learning Representations*, 2024a.

Liu, H., Li, C., Li, Y., and Lee, Y. J. Improved baselines with visual instruction tuning. In *Proceedings of the IEEE/CVF Conference on Computer Vision and Pattern Recognition (CVPR)*, pp. 26296–26306, June 2024b.

Liu, H., Li, C., Wu, Q., and Lee, Y. J. Visual instruction tuning. *Advances in Neural Information Processing Systems*, 36, 2024c.

Liu, H., Xue, W., Chen, Y., Chen, D., Zhao, X., Wang, K., Hou, L., Li, R., and Peng, W. A survey on hallucination in large vision-language models. *arXiv preprint arXiv:2402.00253*, 2024d.

Lu, J., Batra, D., Parikh, D., and Lee, S. Vilbert: Pretraining task-agnostic visiolinguistic representations for vision-and-language tasks. In *Advances in Neural Information Processing Systems (NeurIPS)*, volume 32, 2019.

Mukhoti, J., Kulharia, V., Sanyal, A., Golodetz, S., Torr, P., and Dokania, P. Calibrating deep neural networks using focal loss. *Advances in Neural Information Processing Systems*, 33:15288–15299, 2020.

Nie, J., Zhang, G., An, W., Tan, Y.-P., Kot, A. C., and Lu, S. Mmrel: A relation understanding dataset and benchmark in the mllm era. *arXiv preprint arXiv:2406.09121*, 2024.

Peng, Z., Wang, W., Dong, L., Hao, Y., Huang, S., Ma, S., and Wei, F. Kosmos-2: Grounding multimodal large language models to the world. *arXiv preprint arXiv:2306.14824*, 2023.

Platt, J. C. Probabilistic outputs for support vector machines and comparisons to regularized likelihood methods. In *Advances in Large Margin Classifiers*, pp. 61–74. MIT Press, 1999.

Radford, A., Kim, J. W., Hallacy, C., Ramesh, A., Goh, G., Agarwal, S., Sastry, G., Askell, A., Mishkin, P., Clark, J., Krueger, G., and Sutskever, I. Learning transferable visual models from natural language supervision. In *Proceedings of the International Conference on Machine Learning*, pp. 8748–8763. PMLR, July 2021.

Raffel, C., Shazeer, N., Roberts, A., Lee, K., Narang, S., Matena, M., Zhou, Y., Li, W., and Liu, P. J. Exploring the limits of transfer learning with a unified text-to-text transformer. *The Journal of Machine Learning Research*, 21(1):5485–5551, 2020.

Rohrbach, A., Hendricks, L. A., Burns, K., Darrell, T., and Saenko, K. Object hallucination in image captioning. In *Proceedings of the 2018 Conference on Empirical Methods in Natural Language Processing (EMNLP)*, pp. 4035–4045, 2018.

Schwenk, D., Khandelwal, A., Clark, C., Marino, K., and Mottaghi, R. A-okvqa: A benchmark for visual question answering using world knowledge. In *European Conference on Computer Vision*, pp. 146–162. Springer, 2022.

Shang, Y., Cai, M., et al. Llava-prumerge: Adaptive token reduction for efficient large multimodal models. *arXiv preprint arXiv:2403.15388*, 2024.

Sun, Z., Shen, S., Cao, S., Liu, H., Li, C., Shen, Y., Gan, C., Gui, L., Wang, Y.-X., Yang, Y., et al. Aligning large multimodal models with factually augmented rlhf. *arXiv preprint arXiv:2309.14525*, 2023.

Tan, H. and Bansal, M. Lxmert: Learning cross-modality encoder representations from transformers. *arXiv preprint arXiv:1908.07490*, 2019.

Taori, R., Gulrajani, I., Zhang, T., Dubois, Y., Li, X., Guestrin, C., Liang, P., and Hashimoto, T. B. Stanford alpaca: An instruction-following llama model, 2023. [https://github.com/tatsu-lab/stanford\\_alpaca](https://github.com/tatsu-lab/stanford_alpaca).

Touvron, H., Martin, L., and et al. Llama 2: Open foundation and fine-tuned chat models. *arXiv preprint arXiv:2307.09288*, 2023.

Wang, X., Zhou, Y., Liu, X., Lu, H., Xu, Y., He, F., Yoon, J., Lu, T., Bertasius, G., Bansal, M., et al. Mementos: A comprehensive benchmark for multimodal large language model reasoning over image sequences. *arXiv preprint arXiv:2401.10529*, 2024.

Wu, Z., Xiong, Y., Yu, S. X., and Lin, D. Unsupervised feature learning via non-parametric instance discrimination. In *Proceedings of the IEEE Conference on Computer Vision and Pattern Recognition*, pp. 3733–3742, 2018.

Xing, Y., Li, Y., Laptev, I., and Lu, S. Mitigating object hallucination via concentric causal attention. *arXiv preprint arXiv:2410.15926*, 2024.

Ye, Q., Xu, H., Ye, J., Yan, M., Hu, A., Liu, H., et al. Mplug-owl2: Revolutionizing multi-modal large language model with modality collaboration. In *Proceedings of the IEEE/CVF Conference on Computer Vision and Pattern Recognition (CVPR)*, pp. 13040–13051, 2024.

Yin, S., Fu, C., Zhao, S., Xu, T., Wang, H., Sui, D., Shen, Y., Li, K., Sun, X., and Chen, E. Woodpecker: Hallucination correction for multimodal large language models. *arXiv preprint arXiv:2310.16045*, 2023.

You, H., Zhang, H., Gan, Z., Du, X., Zhang, B., Wang, Z., Cao, L., Chang, S.-F., and Yang, Y. Ferret: Refer and ground anything anywhere at any granularity. *arXiv preprint arXiv:2310.07704*, 2023.

Yu, Q., Li, J., Wei, L., Pang, L., Ye, W., Qin, B., and Zhuang, Y. Hallucidoctor: Mitigating hallucinatory toxicity in visual instruction data. In *Proceedings of the IEEE/CVF Conference on Computer Vision and Pattern Recognition*, pp. 12944–12953, 2024.

Zhang, S., Sun, P., Chen, S., Xiao, M., Shao, W., Zhang, W., Chen, K., and Luo, P. Gpt4roi: Instruction tuning large language model on region-of-interest. *arXiv preprint arXiv:2307.03601*, 2023a.

Zhang, Y., Qian, S., Peng, B., Liu, S., and Jia, J. Prompt highlighter: Interactive control for multi-modal llms. *arXiv preprint arXiv:2312.04302*, 2023b.

Zhou, Y., Cui, C., Yoon, J., Zhang, L., Deng, Z., Finn, C., Bansal, M., and Yao, H. Analyzing and mitigating object hallucination in large vision-language models. In *The Twelfth International Conference on Learning Representations*, 2024.

Zhu, D., Chen, J., Shen, X., Li, X., and Elhoseiny, M. Minigpt-4: Enhancing vision-language understanding with advanced large language models. *arXiv preprint arXiv:2304.10592*, 2023.

## A. Additional Experimental Settings

**Evaluation Setup** For comparison, we adopt the default settings for OPERA, VCD, and SID. For CCA, we directly use the provided weights. For polling-based tasks (POPE and MME), we employ greedy decoding, while for open-ended generation tasks (CHAIR and LLaVA-Bench), we utilize sampling with  $\text{Top-}p = 1$ .

**DAC Training** For implementing DAC on LLaVA-1.5, we set the learning rate to  $3 \times 10^{-6}$ . For LLaVA-NeXT, the learning rate is set to  $8 \times 10^{-7}$ , while for mPLUG-Owl2, we use a learning rate of  $3 \times 10^{-5}$ .

The application of DAC varies across models. For LLaVA-1.5 and LLaVA-NeXT, DAC is applied to the last token before prediction. In contrast, for mPLUG-Owl2, DAC is applied to all tokens after the image starting position. For LLaVA-1.5 and LLaVA-NeXT, DAC consists of two layers with a hidden dimension of 576, which matches both the input and output dimensions. For mPLUG-Owl2, DAC is set to three layers with a hidden dimension of 576 to maintain a similar capacity.

## B. SPB on other blank images

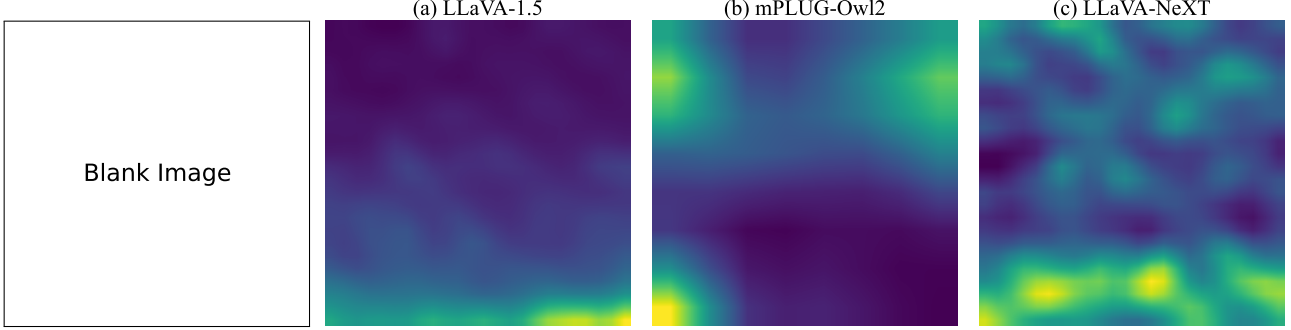


Figure 3: Vision tokens attention weights during the decoding process for different models on a blank white image in response to the polling prompt: “Is there a bear in the image?”

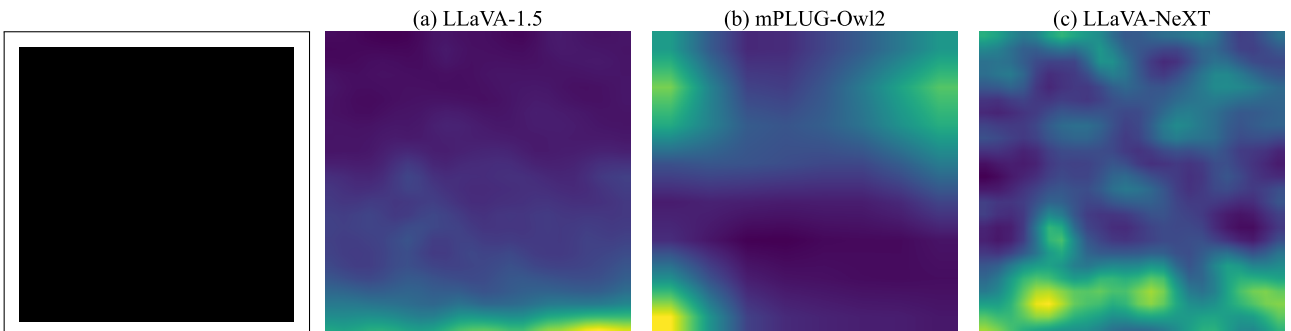


Figure 4: Vision tokens attention weights during the decoding process for different models on a blank black image in response to the polling prompt: “Is there a bear in the image?”

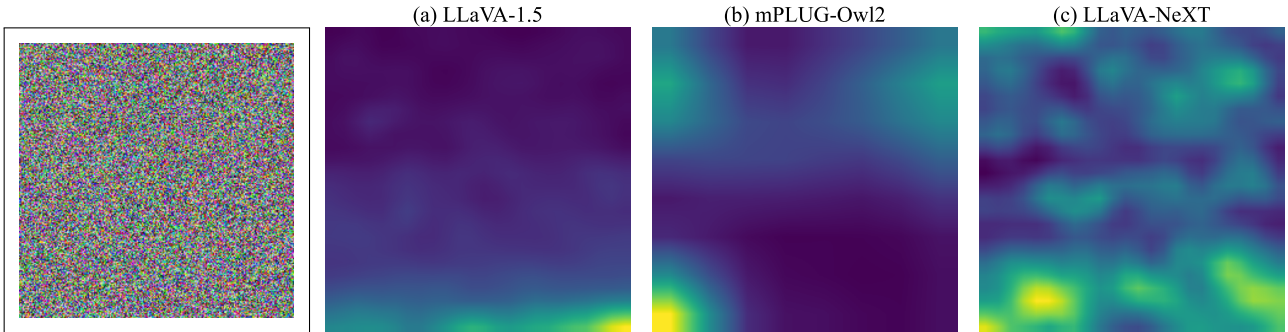


Figure 5: Vision tokens attention weights during the decoding process for different models on a blank noise image in response to the polling prompt: “Is there a bear in the image?”

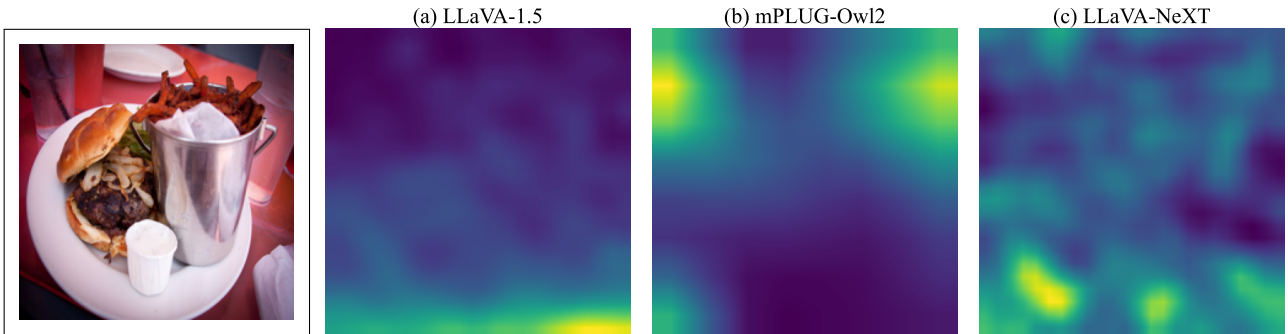


Figure 6: Vision tokens attention weights during the decoding process for different models on an actual image in response to the polling prompt: “Is there a bear in the image?”

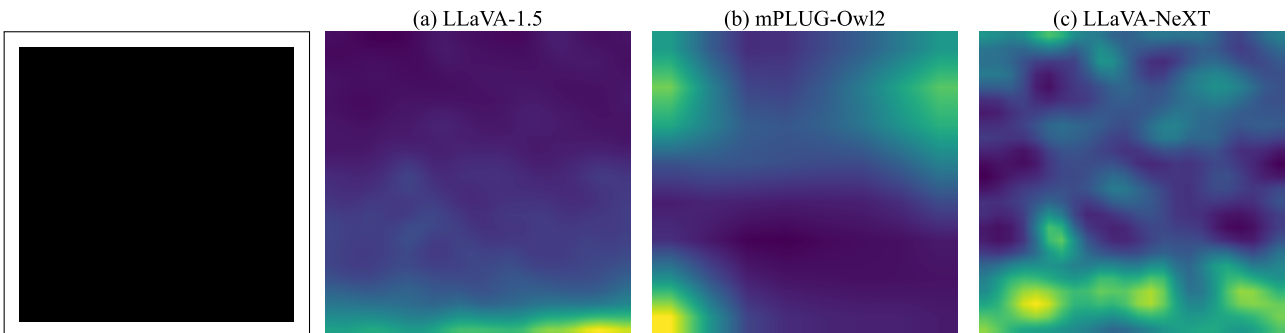


Figure 7: Vision tokens attention weights during the decoding process for different models on a blank black image in response to the open-ended prompt: “Please describe the image in detail.”

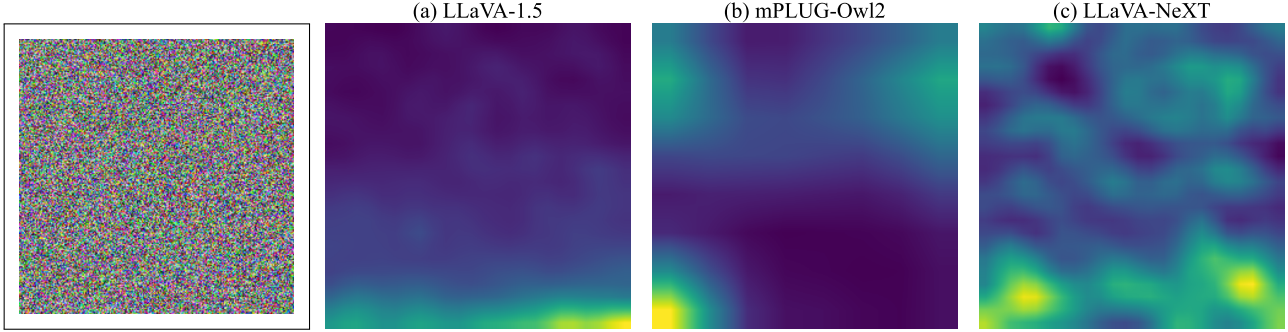


Figure 8: Vision tokens attention weights during the decoding process for different models on a blank noise image in response to the open-ended prompt: “Please describe the image in detail.”

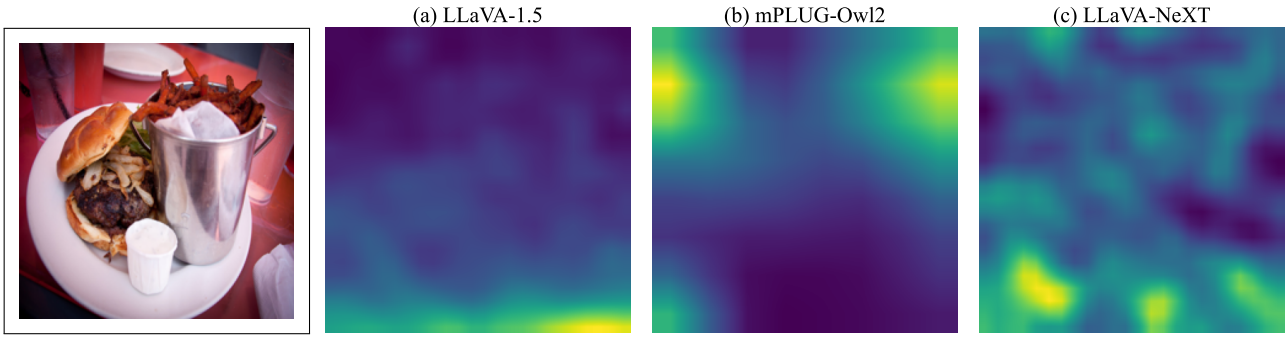


Figure 9: Vision tokens attention weights during the decoding process for different models on an actual image in response to the open-ended prompt: “Please describe the image in detail.”

### C. DAC architecture

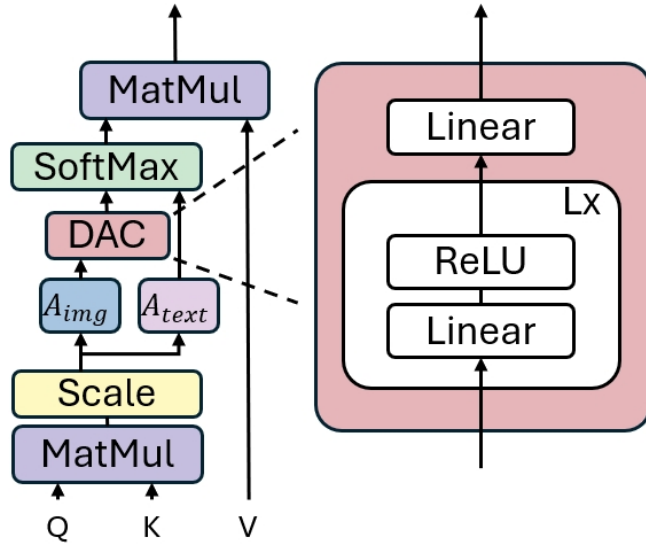


Figure 10: The Dynamic Attention Calibration (DAC) architecture consists of a small stack of linear transformations with ReLU activation, operating within the self-attention mechanism of transformer decoder layers to calibrate vision tokens attention.

## D. Data Augmentation Process

The augmentation process consists of the following steps:

- For each annotated object in  $V$ :
  - Crop the region defined by its bounding box.
  - Randomly resize the cropped object to a minimum size of  $(H/14) \times (W/14)$  pixels (the typical size of an image patch) and a maximum size of  $(H/2) \times (W/2)$ , where  $H$  and  $W$  are the height and width of the original image  $V$ .
  - Replace the background of the cropped object with pure white, resulting in  $V_{\text{crop}}$
- For each cropped object  $V_{\text{crop}}$ :
  - Generate a corresponding positive query  $T_{\text{pos}}$  that describes the cropped object and assign the label  $Y_{\text{pos}} = \text{yes}$ .  
Obtaining positive query-label pair:  $(T_{\text{pos}}, V_{\text{crop}}, Y_{\text{pos}})$
  - Generate a ground-truth negative query  $T_{\text{neg}}$ , which refers to an object not present in the image, and assign the label  $Y_{\text{neg}} = \text{no}$ .  
Obtaining negative query-label pair:  $(T_{\text{neg}}, V_{\text{crop}}, Y_{\text{neg}})$
  - Each cropped image  $V_{\text{crop}}$  results in one positive query-label pair and one negative query-label pair, ensuring a balanced augmented set.

Let  $I$  represent the number of original images in the calibration set  $\mathcal{D}_{\text{cal}}$ ,  $J$  represent the average number of annotated ground-truth objects per image  $V$ , and  $K$  represent the number of crops generated per object. The total size of the augmented dataset is: Total size of  $\mathcal{D}_{\text{aug}} = I \cdot J \cdot K \cdot 2$

---

### Algorithm 2 Data Augmentation Algorithm

---

**Input:** Calibration set  $\mathcal{D}_{\text{cal}} = \{(T_i, V_i, Y_i)\}_{i=1}^I \subset \mathcal{D}_{\text{val}}$   
 $I$ : Size of calibration set  
 $J$ : Number of annotations per image  
 $K$ : Number of crops per object  
 Augmented set  $\mathcal{D}_{\text{aug}} = \{\}$   
**for**  $i = 1$  to  $I$  **do**  
     **for**  $j = 1$  to  $J$  **do**  
         **for**  $k = 1$  to  $K$  **do**  
             Get  $V_{\text{crop}}$  for object  $j$   
             Assign  $(T_{\text{pos}}, V_{\text{crop}}, Y_{\text{pos}})$   
             Assign  $(T_{\text{neg}}, V_{\text{crop}}, Y_{\text{neg}})$   
             Append both pairs to  $\mathcal{D}_{\text{aug}}$   
         **end for**  
     **end for**  
**end for**  
**Return:**  $\mathcal{D}_{\text{aug}} = \{(T_{\text{aug}}, V_{\text{crop}}, Y_{\text{aug}})\}$  with size  $I \cdot J \cdot K \cdot 2$

---

## E. Additional Experimental Results

Method	Perception										Total
	existence	count	position	color	posters	celebrity	scene	landmark	artwork	OCR	
UAC	190	155	128.3	165	145.6	136.5	158.8	163.8	124	142.5	1509.4
DAC	195	158.3	133.3	170	140.5	131.2	161.5	165.5	123.3	137.5	1516.0

Table 6: Results on full **MME Perception** subsets

Method	Commonsense Reasoning	Numerical Calculation	Text Translation	Code Reasoning	Total
UAC	117.14	70	115	57.5	359.6
DAC	121	57.5	85	80	343.9

Table 7: Results on full **MME Cognition** subsets